Model reduction for nonlinear aeroelasticity using the Discrete Empirical Interpolation Method

Model reduction for nonlinear aeroelasticity using the Discrete Empirical nterpolation Method

Yao, W., & Marques, S. (2016). Model reduction for nonlinear aeroelasticity using the Discrete Empirical nterpolation Method. Paper presented at Royal Aeronautical Society 5th Aircraft Structural Design Conference, Manchester, United Kingdom.

Model reduction for nonlinear aeroelasticity using the Discrete Empirical Interpolation Method

W. Yao
mpeyaow@nus.edu.sg
National University of Singapore
Department of Mechanical Engineering
Singapore
Singapore

S. Marques
Queen's University Belfast
School of Mechanical and Aerospace Engineering
Belfast
U.K.

ABSTRACT

A novel surrogate model is proposed in lieu of computational fluid dynamic (CFD) code for fast nonlinear aerodynamic modeling. First, a nonlinear function is identified on selected interpolation points defined by discrete empirical interpolation method (DEIM). The flow field is then reconstructed by a least square approximation of flow modes extracted by proper orthogonal decomposition (POD). The proposed model is applied in the prediction of limit cycle oscillation for a plunge/pitch airfoil and a delta wing with linear structural model, results are validate against a time accurate CFD-FEM code. The results show the model is able to replicate the aerodynamic forces and flow fields with sufficient accuracy while requiring a fraction of CFD cost.

.

NOMENCLATURE

$\mathbf{A}$	matrix of snapshots
b, c	aerofoil semi-chord and chord, respectively
c_i	radial basis function artificial neural network neuron i center
C_L	lift coefficient
C_N	normal force coefficient
C_M	pitching moment coefficient
$\mathbf{f}$	fluid force acting on structure
$\mathbf{H}$	radial basis function design matrix
h	plunge coordinate
h_{ij}	radial basis function for snapshot i with respect to neuron j
$\mathbf{K}$	structure stiffness matrix
$\mathbf{M}$	structure mass matrix
M_∞	free-stream Mach number
M	number of POD basis retained
$\mathbf{P}$	interpolation indices matrix
n	number of delayed displacements recorded
q	dynamic pressure
$\mathbf{R}$	vector of fluid and structural equations residuals
r_i	radial basis function artificial neural network neuron i radius
$\mathbf{S}$	diagonal matrix containing singular values
t	time
$\mathbf{T}$	matrix of POD basis
$U_\infty, \mathbf{U}$	free-stream velocity, velocity vector, respectively
$\mathbf{u}$	variable for model reduction process
V_s	reduced velocity index
$\mathbf{w}$	vector of fluid and structural unknowns
$\mathbf{x}$	list of displacements

Greek Symbol

α	angle of attack
$\mathbf{\Phi}$	radial basis function artificial neural network weights vector
ω, κ	frequency and reduced frequency, $\kappa = \frac{2\omega}{U_\infty c}$
φ	phase angle
ρ	fluid density
$\boldsymbol{\xi}$	structural displacement

1.0 Introduction

Computational fluid dynamics (CFD) has become a critical technique for several engineering applications, including aerospace, chemical, automotive engineering, among others. Despite the ever increasing computer power available, high computational cost still prevents state-of-art CFD to be routinely used in procedures where iterative processes are intrinsic such as design/optimization, combustion, uncertainty quantification, and more pertinent to this work

dynamic aeroelasticity. To overcome the need for time-accurate CFD, there has been a continuous interest in developing efficient and accurate techniques that avoid the penalty of full blown time-accurate CFD simulations.

In the context of dynamic aeroelasticity, several advances have been made. If the system Jacobians are available, it is possible to determine the stability of the dynamic system (i.e. flutter boundary) without resorting to time-domain simulations by eigenvalue analysis[1], in addition a nonlinear reduced-order model can be built to compute LCOs, by further exploiting the aeroelastic critical eigenvector[19].

The prediction of LCO can also be achieve by exploiting the periodicity of the CFD-CSD (Computational Structural Dynamics) system using the so called harmonic-balance method[21], which solves directly the periodic response directly. The application of the aforementioned methods requires significant modifications to existing codes. To limit any required modifications, surrogate models based on samples or snapshots from CFD analysis can be built. Several techniques have been proposed for linear modeling, or only retaining the linear part of the original CFD system: system identification (ID) or modal superimposition methods such as Volterria Series[20,2], POD[7,14] and Balanced Proper Orthogonal Decomposition[18,25].

Building a nonlinear ROM poses a more significant challenge and is the subject of much attention within the modeling community. Hence, several nonlinear ROMs have been developed and applied successfully as nonlinear surrogates, for example: *Artificial Neural Network Auto-Regressive Exogenous* (ANN-ARX)[5,31], K*riging-ARX*[6],*Continuous Time Recurrent Neural Network*[15]. The nonlinear models proposed in references[31,6,15] are built using the pitching angle or structural displacements as input and the aerodynamic force as output, however the models are not able to provide flow field information, such as pressure. Fagley *et al.* used POD and ANN-ARX to investigate the free shear layer transient effects[5]. Following the same idea, Lindhorst *et al.* employed POD with a Markov-Chain interpolator function and Radial-Basis Function Artificial Neural Network (RBF-ANN) to model nonlinear aerodynamic flows for aero-structural calculations, in this approach the input and output were the POD coefficients of the grid displacement and aerodynamic force distribution[11,12], the authors also suggested that excessive POD modes may degrade the approximation accuracy. Recently, Yao and Marques proposed an alternative approach based on a POD/DEIM model reduction technique able to reconstruct the nonlinear flow field from the structural displacements;[29] the following section will summarize this method and investigate its ability to predict LCOs at a reduced cost.

2.0 Formulation

As discussed in the introduction, the purpose of the ROM is to reduce the effort associated with high-fidelity unsteady aerodynamic calculations required for aeroelastic predictions. Typical CFD/CSD solvers exchange information in the form of displacements, velocities and pressures, hence the point of the surrogate model is to provide the surface pressure (or equivalent) associated with any translations or rotations from the structure. For that purpose, it is possible to define a nonlinear mapping between inputs and outputs that can replace the discrete full order CFD/CSD system[26]:

$$\mathbf{Q}_f(t) = \mathcal{F}\left(\mathbf{w}_s(t), \mathbf{w}_s(t-\Delta t), \mathbf{w}_s(t-2\Delta t), \ldots, \mathbf{w}_s(t-n\Delta t)\right) \tag{1}$$

where $\mathbf{Q}_f$ represents fluid variables such as pressure or temperature; $\mathbf{w_s} = \left[\boldsymbol{\xi}, \dot{\boldsymbol{\xi}}\right]$ are the structural displacement and velocity. The inputs to the nonlinear function $\mathcal{F}$, is the structural displacement and its delay and the fluid variables are the output. In practice, the surrogate only approximates $\mathcal{F}$. To build the surrogate, the following steps are required:

1. generate an adequate training trajectory covering the parameter space of interest;
2. collect snapshots along the training trajectory of the full-order model (FOM) response;
3. compute POD modes;
4. apply DEIM to POD modes and determine interpolation points;
5. build RBF-ANN for each interpolation point;

then, using the RBF-ANN and designated interpolation points, it is possible to reconstruct the whole flow field using the DEIM and to integrate the surface pressure to determine the aerodynamic loads for the structural solver.

2.1 Time-Domain Fluid-Structural Solver

To obtain the snapshots required to build the ROM, a research CFD-FEM (Finite Element Model) code is used. The aerodynamic model is based on the Euler equations for fluid flow and as is typical in computational aeroelasticity a modal structural model is used to represent the structure. The discretization of the fluid fluxes is obtained using the $AUSM^+ - up$ flux function;[13] a MUSCL scheme together with the Van Albada limiter is employed to achieve 2^{nd} order spatial accuracy in smooth regions[23]. The scheme is marched forward in time using a dual-time-stepping strategy, four-stage Runge-Kutta scheme[27]. The structural equations are transformed into a state-space representation, involving the generalized aerodynamic forces from the fluid system[22,27]. For wing structures, the aerodynamic loads and structural displacements transfers between the CFD/FEM are obtained through the Infinite Plate Spline (IPS) method. Transfinite Interpolation is used to deform the CFD mesh and grid velocities are approximated using finite-differences.

2.2 Proper Orthogonal Decomposition

The use of POD as a means of reducing the complexity of large dynamic systems described by partial-differential equations extends to several engineering applications.[3] In this work, the POD modes (also referred to as POD basis) of the CFD system are sought. For a set of snapshots of the flow field, $\mathbf{A} = [\mathbf{u}_1, \mathbf{u}_2, \ldots, \mathbf{u}_{n_s}]$, the POD basis represents an optimal set of orthogonal vectors that can best approximate the snapshots. The snapshots are obtained from the time-accurate CFD/CSD solution and are recorded at specified time instances. For the current applications, only the pressure field is recorded, hence each snapshot is a vector $\mathbf{u} \in \mathbb{R}^{n_c \times 1}$, where n_c is the number of cells in the CFD mesh, making $\mathbf{A} \in \mathbb{R}^{n_c \times n_s}$. A well known method to obtain the POD basis of $\mathbf{A}$ is to compute its left singular vectors by singular value decomposition (SVD), however for large systems where $n_s < n_c$, then the SVD is applied to $\mathbf{A}^T\mathbf{A} \in \mathbb{R}^{n_s \times n_s}$:

$$\mathbf{A}^T\mathbf{A} = \mathbf{T}\mathbf{S}\mathbf{V}^T \tag{2}$$

where $\mathbf{S} = diag\left[\lambda_1, \lambda_2, \ldots, \lambda_{n_s}\right]$ is the eigenvalue matrix and $\mathbf{T}, \mathbf{V}$ are the left and right singular vectors, respectively. The POD basis, $\mathbf{T}_M \in \mathbb{R}^{n_c \times M}$, is obtained from Eq. (3) with

proper truncation according to the energy rank represented by the amplitude of the first M eigenvalues, $\mathbf{S}_M = diag\,[\lambda_1, \lambda_2, \ldots, \lambda_M]$, where $\lambda_1 > \lambda_2 > \ldots > \lambda_M$ and $M \ll n_c$.

$$\mathbf{T}_M = \mathbf{A}\mathbf{V}\mathbf{S}_M^{-1/2} \tag{3}$$

2.3 Discrete Empirical Interpolation Method

In this section, the DEIM is reviewed. The application of POD is limited to linear or mildly nonlinear time or parameter dependent system of partial-differential equations[16]. As nonlinearities become dominant, its efficiency deteriorates, rendering the use of POD unattractive for nonlinear aeroelastic problems. In this paper DEIM is used to overcome this limitation. In essence DEIM approximates a parametric nonlinear function, $\mathbf{u}(t)$, by projecting it onto the subspace spanned by the basis $\mathbf{T}_M$ as:

$$\mathbf{u}(t) \approx \mathbf{T}_M \mathbf{c}(t) \tag{4}$$

where $\mathbf{c}(t) \in \mathbb{R}^{M\times 1}$ are the corresponding coefficients. The methodology proposed by Chaturantabut *et al.* enables selecting M distinct rows or interpolation indices so that the coefficients $\mathbf{c}(t)$ can be solved uniquely as described in[4]. The interpolation indices are defined by the matrix $\mathbf{P} \in \mathbb{R}^{n_c\times M}$, where each row contains interpolation indices, which leads to

$$\mathbf{P}^T\mathbf{u}(t) = \mathbf{P}^T\mathbf{T}_M\mathbf{c}(t) \tag{5}$$

Substituting Eq. 5 into Eq. 4, obtain:

$$\mathbf{u}(t) \approx \mathbf{T}_M \left(\mathbf{P}^T\mathbf{T}_M\right)^{-1} \mathbf{P}^T\hat{\mathbf{u}}(t) \tag{6}$$

where $\hat{\mathbf{u}}(t)$ contains the components corresponding to non-zeros indices in $\mathbf{P}$, hence Eq.6 shows that M elements are required to recover the full order vector $\mathbf{u}(t)$. For fluid systems, let $\mathbf{u}(t)$ represent the pressure field. As described in Eq. 1, the nonlinear mapping function $\mathcal{F}$ can be constructed at M interpolation points. The full order vector $\mathbf{u}(t)$ is reconstructed by Eq. 6.

2.4 Radial Basis Function - Artificial Neural Network

The nonlinear mapping function in Eq. 1 is defined by an RBF-ANN. The input/output is at user's discretion according to the specific physical problem at hand. In the present paper, the input and output are displacements and pressures from the structure and fluid, respectively. The idea is to construct the RBF-ANN of the pressure at M interpolation points defined by the DEIM algorithm. The neuron is modeled by RBFs as[17]

$$h_i = e^{-\frac{|x(t) - c_i|^2}{r_i}}, i = 1, 2, \ldots, M \tag{7}$$

where c_i and r_i are the ith neuron centre and radius, respectively; $\mathbf{x}$ is the input, given by

$$\mathbf{x}(t) = [\boldsymbol{\xi}(t), \boldsymbol{\xi}(t - \Delta t), \ldots, \boldsymbol{\xi}(t - n\Delta t)] \tag{8}$$

In this work *even evolving input data* is chosen to provide the RBF center c_i, due to its simplicity. The radius r_i or width is defined as per reference[11]:

$$r_i = \frac{1}{M}\sum_{j=1}^{M} \|c_j - c_i\|^2, i = 1, 2, \ldots, M \tag{9}$$

Once c_i and r_i are identified, the training process can be completed. The mapping relation between inputs and outputs is obtained by a weighted sum; the function weights $\mathbf{\Phi}$ are obtained using the target flow variables defined by $\hat{\mathbf{u}}$, at the interpolation points:

$$\hat{\mathbf{u}} = \mathbf{H}\mathbf{\Phi} \tag{10}$$

where

$$\hat{\mathbf{u}} = [u_1, u_2, \ldots, u_M]^T, \quad \mathbf{\Phi} = [\phi_1, \phi_2, \ldots, \phi_M]^T \tag{11}$$

and

$$\mathbf{H} = \begin{bmatrix} h_{11} & \ldots & h_{1M} \\ \vdots & \ddots & \vdots \\ h_{M1} & \ldots & h_{MM} \end{bmatrix} \tag{12}$$

The weight matrix $\mathbf{\Phi}$ can be solved as,

$$\mathbf{\Phi} = \mathbf{H}^{+}\hat{\mathbf{u}} \tag{13}$$

$\mathbf{\Phi}^{+}$ is the Moore-Penrose pseudo inverse. To avoid possible over fitting and instabilities, a weight penalty or a regularization parameter ε is introduced that is given by[17]:

$$\mathbf{H}^{+} = \left(\mathbf{H}^T\mathbf{H} + \varepsilon\mathbf{I}\right)^{-1}\mathbf{H}^T \tag{14}$$

the parameter ε is a small number, however, it has no optimal value, and is problem dependent. The two and three dimensional cases presented below also adopt the value $\varepsilon = 10^{-7}$.

3.0 Results

3.1 Two degree-of-freedom aeroelastic system

In this section, the ability of the ROM to predict the impact of aerodynamic nonlinearities, i.e. shocks, on aeroelastic stability will be investigated by using a pitch/plunge symmetric NACA 64A010 airfoil, as described in reference[21] and shown in Figure 1. The non-dimensional

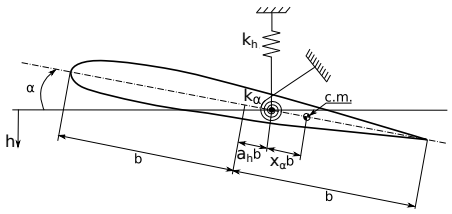

Figure 1. Diagram of pitch/plunge airfoil system.

form of the governing equations of motion for a two degree-of-freedom aerofoil can be described as

$$\mathbf{M}\ddot{\boldsymbol{\xi}} + \frac{1}{\mu V_s^2}\mathbf{K}\boldsymbol{\xi} = \frac{4}{\pi\mu}\mathbf{f} \tag{15}$$

Table 1
Pitch/Plunge Aerofoil Parameters.

Static unbalance, $x_\alpha = S_\alpha/mb$	0.25
Radius of gyration about elastic axis, $r_\alpha^2 = I_\alpha/mb^2$	0.75
Frequency ratio, ω_h/ω_α	0.5
Mass ratio, $\mu = m/\pi\rho_\infty b^2$	75

where

$$\mathbf{M} = \begin{bmatrix} 1 & x_\alpha \\ x_\alpha & r_\alpha^2 \end{bmatrix}, \quad \mathbf{K} = \begin{bmatrix} \left(\frac{\omega_h}{\omega_\alpha}\right)^2 & 0 \\ 0 & r_\alpha^2 \end{bmatrix}, \quad \mathbf{f} = \begin{bmatrix} -C_l \\ 2C_m \end{bmatrix}, \quad \boldsymbol{\xi} = \begin{bmatrix} \frac{h}{b} \\ \alpha \end{bmatrix}, \quad V_s = \frac{U_\infty}{\omega_\alpha b\sqrt{\mu}} \tag{16}$$

the structural parameters are given in Table 1, where S_α, I_α are the first and second moment of inertia about the elastic axis, respectively, m is the mass of the airfoil, ω_h and ω_α are the plunge and pitch motion frequencies, respectively.

The Mach number and angle of attack are 0.8 and 0°, respectively. The velocity index, V_s, is used to set different instability points, i.e. flutter and LCO conditions. The training trajectory is defined using a single input, V_s, according to

$$V_s = V_{s0}\left(1 - \delta\sin^2(2\kappa t)\right) \tag{17}$$

To ensure a suitable range of reduced velocities for this case $V_{s0} = 0.8$, $\delta = 0.15$ and $\kappa = 0.015$, this results in the range $0.68 \leq V_s \leq 0.8$, which includes the flutter onset velocity, $V_s = 0.71$ [27], and a suitable range of post-critical velocities. The resultant training trajectory with a relative large plunge perturbation is shown in Figure 2-(a) and the corresponding range of frequencies of the settled down part of the trajectory is illustrated by the Hilbert-Huang Transformation (HHT) [9] in Figure 2-(b). The user's parameters V_{s0}, δ and κ can be adapted to generate the required training trajectory, as it will be shown in the subsequent test case. Snapshots are collected from the training process and the POD modes extracted following the same procedure described for the forced motion problem. The energy associated with each eigenvalue decays rapidly, as seen in Figure 3-(a). Thirty POD modes are retained and the associated DEIM points used for interpolation are given in Figure 3-(b). The first three POD modes are illustrated in Figure 4. The first mode represents mean flow, the second and the third are POD modes associated with the shock. The inputs to the RBF-ANN are the pitching and plunging displacements at the DEIM points using 4 delays. The ability of the ROM to reconstruct the flow solution is first evaluated by comparing the results for the training trajectory. For both the degrees-of-freedom and aerofoil loads, the ROM is able to recreate the CFD output, see Figure 5. The ROM is then used to evaluate the system's dynamic response at a series of post-critical V_s values. A case near the limit of the training data parameter range, $V_s = 0.775$, is investigated in detail. At this reduced velocity the system develops an LCO and Figure 6 shows the amplitudes for both plunge and pitch; the ROM systematically under predicts both amplitudes by a small margin, it also shows a small delay in reaching the final amplitude of the LCO due to insufficient training points at small amplitudes; the frequency of the motion is well captured. The computational effort required to build the ROM is given in Table 2. Once the ROM is built, each calculation above the critical speed requires approximately 20 seconds.

3.2 Cropped Delta Wing

To further validate the proposed method, a cropped delta wing model is used; the wing uses a *NACA* 65*A*004 airfoil, the leading edge sweep angle is approximately 16° and the semi-span

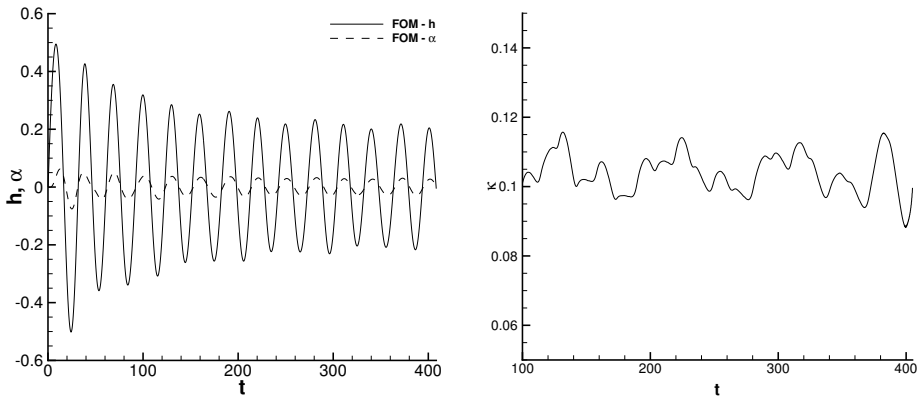

(a) Training trajectory from varying V_s (b) HHT of training trajectory

Figure 2. LCO training trajectory.

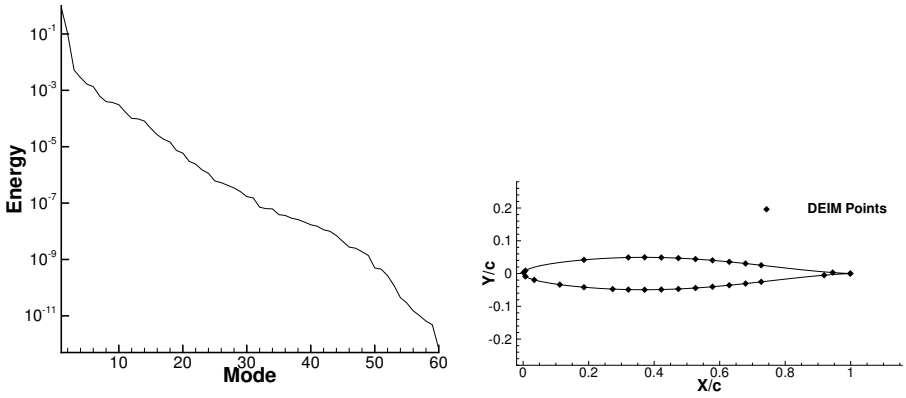

(a) Snapshot matrix eigenvalue decay (b) Location of DEIM points

Figure 3. Snapshot matrix eigenvalue energy and retained DEIM points.

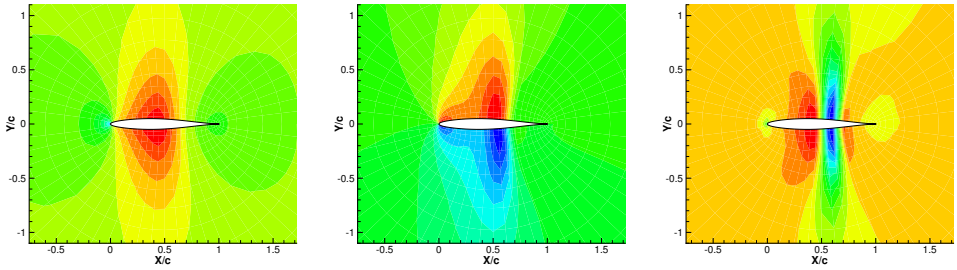

(a) POD Mode 1 (b) POD Mode 2 (c) POD Mode 3

Figure 4. POD modes from pressure flow field.

Table 2
Computational effort to build ROM.

Model	Wall clock [minutes]		
Building ROM	Training Data	DEIM	RBF-ANN
	180.5	0.12	9.95
ROM	0.32		

is just under $4m$. The wing structure is modelled using 2D shell elements and the material properties are based on the AGARD 445.6 wing[30]. Further details of the wing structural dynamics and aeroelastic characteristics can be found in references[27,29], where it was found the wing exhibited LCOs at transonic conditions, Mach number of 0.91 and 0° angle-of-attack, due to the motion of the shock located near the trailing edge. As before, the ROM

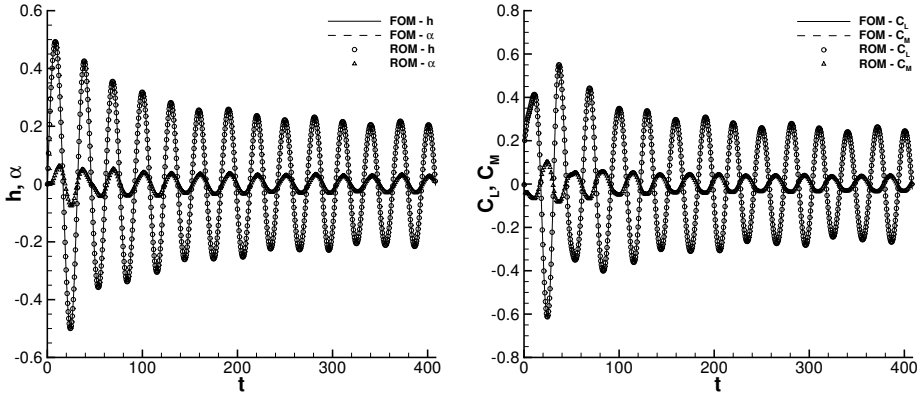

(a) Training trajectory displacements (b) Training trajectory loads

Figure 5. Training data evaluation.

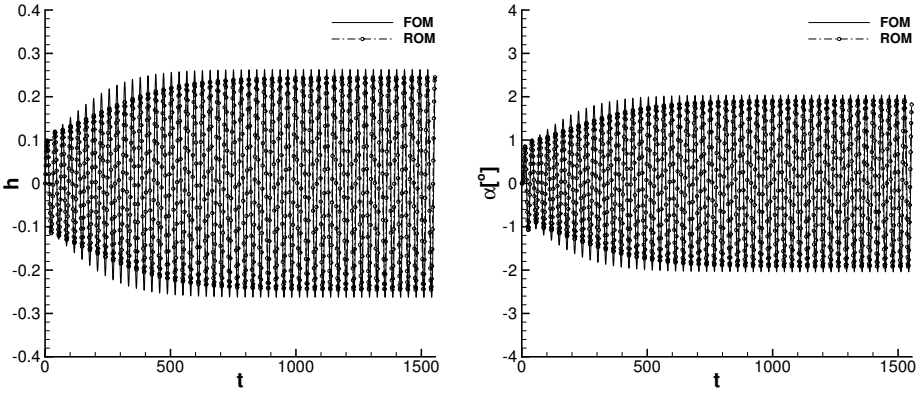

(a) Plunge displacement (b) Pitch displacement

Figure 6. LCO time history comparison of CFD and ROM.

first requires building the training trajectory, which in this case is generated by varying the dynamic pressure q as

$$q = q_0 \left(1 - \delta \sin^2 (2\kappa t)\right) \tag{18}$$

where $q_0 = 0.873 q_{sl}$ which is 15% above the flutter onset conditions (q_f) and q_{sl} is the dynamic pressure at sea level conditions, the remainder parameters are: $\delta = 0.15$ and $\kappa = 0.01$. The final training trajectory obtained is shown in Figure 7-(a), where the coordinate η corresponds to the displacement of the wing tip's trailing edge. The HHT results in Figure 7-(b) reveal the range of frequencies covered, ensuring the frequencies of interest are integrated in the training process. Following the two-dimensional aeroelastic case, POD modes were ex-

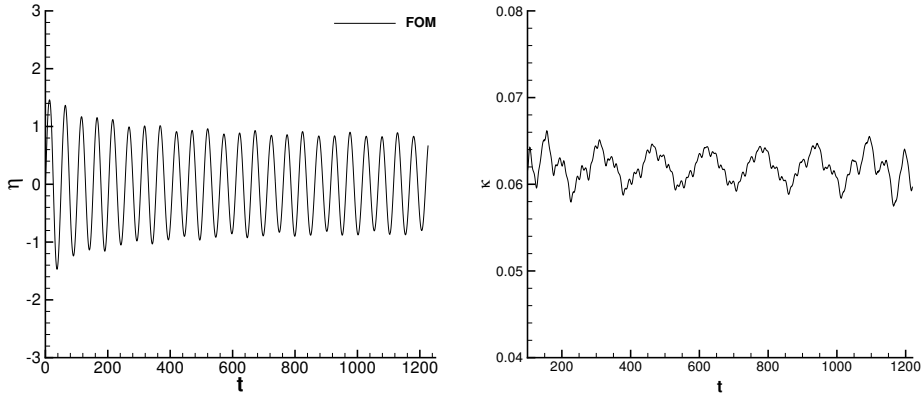

(a) Training trajectory from varying q (b) HHT of training trajectory

Figure 7. LCO training trajectory.

tracted and the eigenvalue history is shown in Figure 8. The first three POD modes are shown in Figure 9(a)-(c), which reveals the first mode to represent the mean flow, the second and the third modes are associated with the shock-wave. Unlike the previous cases, the third mode is now asymmetric. A total of 120 DEIM points are used in this case, as shown in Figure 9-(d). The points cluster near the shock wave location, and regions of large pressure gradients. Again, at each DEIM point the RBF-ANN was identified through the training process. The input for this case are the modal displacements and eight delays are used to obtain satisfactory approximation to the full-order model. The ROM is then constructed using 120 POD modes. The ability of the ROM to replicate the displacement and loads observed in the training trajectory is shown in Figure 10, both frequency and amplitude are well captured by the ROM. To exercise the ROM at post-critical conditions, the dynamic pressure is set 15% higher than the flutter condition. As the oscillations develop, during the downwards motion of the wing the shock at the trailing edge moves rewards and a strong suction peak forms on the wing tip, during the upwards movement the shock moves forward and eventually vanishes, the suction peak at the tip moves to the lower surface and the cycle is reversed and restarted. The reconstructed upper surface pressure field as the wing tip bends downwards is compared against the FOM and shown in Figure 11, indicating the proposed methodology is not hindered by the additional complexity of a three-dimensional problem. The LCO mechanism is well predicted by the ROM as demonstrated by the displacement and lift coefficient comparison given in Figure 12.

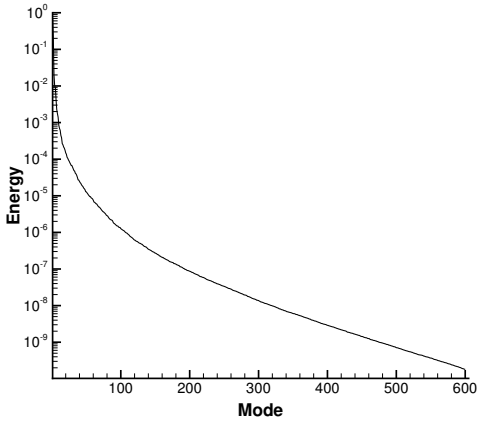

Figure 8. Snapshot matrix eigenvalue energy decay.

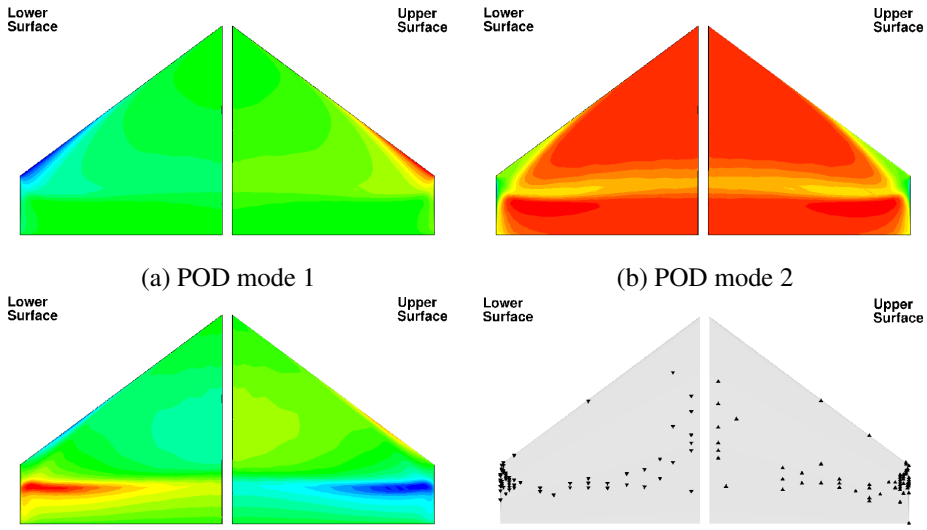

(a) POD mode 1 (b) POD mode 2

(c) POD mode 3 (d) DEIM interpolation points

Figure 9. POD modes from pressure flow field and DEIM interpolation points.

The cost to build and run the ROM is given in Table 3. Each point on the LCO branch takes about one minute to compute using the ROM. The full-order system, using a time step $\Delta t = 10^{-5}$, requires about three-orders of magnitude more effort to run than the ROM at $V_s = 1.15 q_f$. It is reasonable to expect this cost to increase at conditions near the flutter onset, where the number of cycles required to reach the limit-cycle tends to increase.

Table 3
Computational effort to build ROM.

Model	Wall clock [minutes]		
Building ROM	Training Data	DEIM	RBF-ANN
	1224	0.33	88.33
ROM	1.7		

4.0 Conclusions

A novel surrogate model for nonlinear aerodynamic and aeroelastic simulations was demonstrated for LCO prediction. This approach employs a POD/DEIM model reduction technique to problems involving moving boundaries, such as LCOs. The POD/DEIM is able to reduce the full-order aerodynamic system to a very limited number of POD modes and allows reconstructing the complete flow field using information at key locations on the CFD/CSD interface. This ability allows it to be used as a surrogate on behalf of the CFD solver. An RBF-ANN is used to provide a nonlinear mapping between the structure's displacement and the flow quantity of interest used in the reconstruction of the flow field, at the selected CFD/CSD interface points.

The method was exercised using a pith/plunge aeroelastic system which exhibited strong flow nonlinearities in the form of large shock-wave motions. The new ROM was able to capture the main flow features, aerodynamic forces and structural displacements accurately. To highlight the ability of the method in more practical applications, further tests were conducted on a wing geometry, also in the transonic regime. The results obtained further demonstrate the potential of the method to predict LCO amplitudes and frequencies accurately, well beyond the system's bifurcation point.

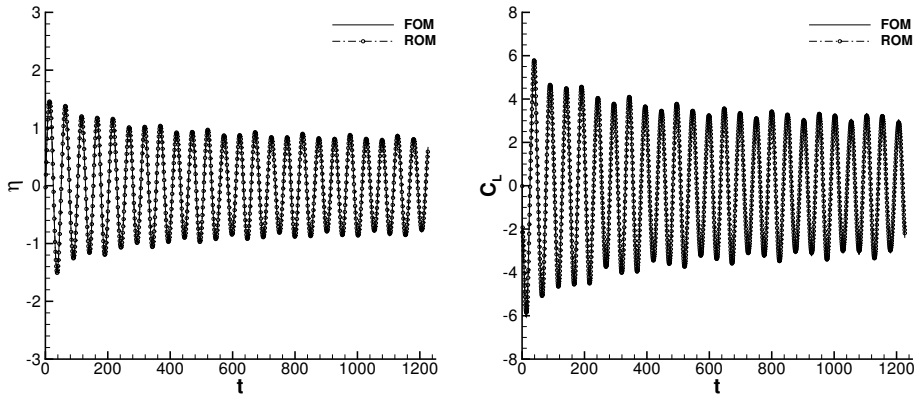

Wing tip displacement Lift coefficient

Figure 10. Wing training trajectory comparison.

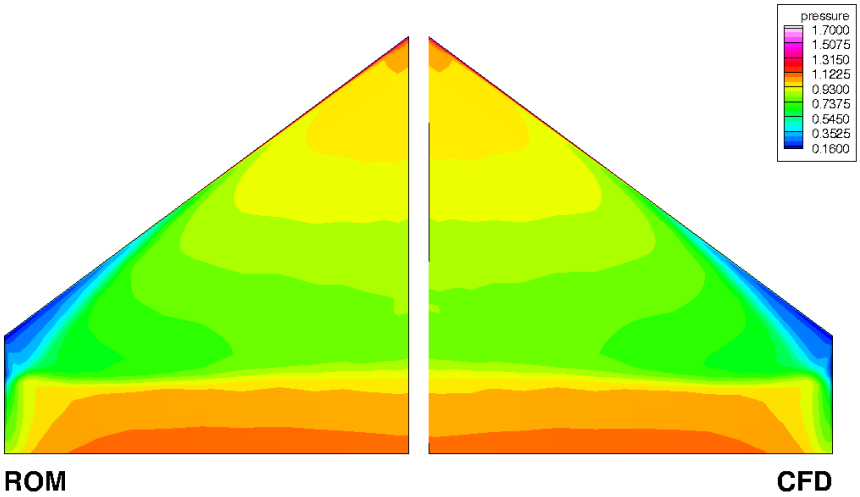

Figure 11. Upper surface pressure field comparison.

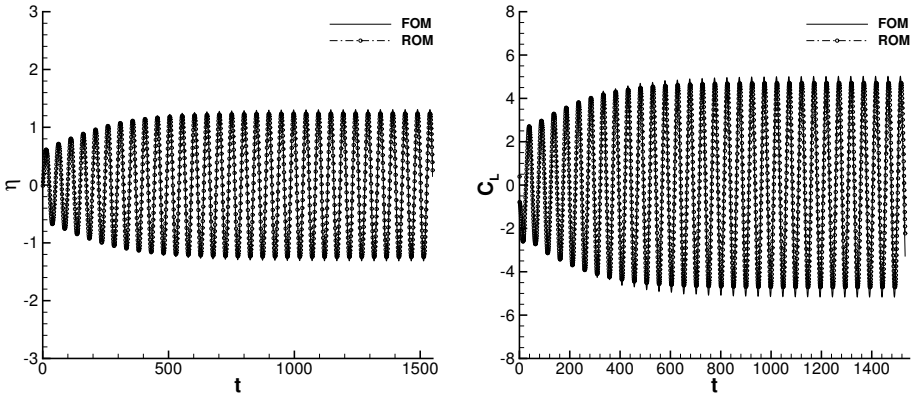

Wing tip displacement Lift coefficient

Figure 12. Wing LCO time history

REFERENCES

1. Badcock, K., Timme, S., Marques, S., Khodaparast, H., Prandina, M., Mottershead, J., Swift, A., Da Ronch, A., and Woodgate, M., Transonic aeroelastic simulation for instability searches and uncertainty analysis, Progress in Aerospace Sciences, Vol. 47, No. 5, (2011), 392–423.
2. Balajewicz, M., and Dowell, E., Reduced-order modeling of flutter and limit-cycle oscillations using the sparse Volterra series, Journal of Aircraft, Vol. 49, No. 6 (2012): 1803–1812.
3. Benner, P., Gugercin, S. and Willcox, K., A survey of projection-based model reduction methods for parametric dynamical systems. SIAM Review vol. 57, No. 4, (2015): 483-531.

4. Chaturantabut, Saifon, and Danny C. Sorensen, Nonlinear model reduction via discrete empirical interpolation, SIAM Journal on Scientific Computing, vol. 32, No. 5, (2010), 2737-2764.
5. Fagley, C., Seidel, J., Siegel, S. and McLaughlin, T., Reduced order modeling using proper orthogonal decomposition (pod) and wavenet system identification of a free shear layer. In Active Flow Control II (pp. 325-339). Springer Berlin Heidelberg, (2010).
6. Glaz, B., Liu, L. and Friedmann, P. P., Reduced-order nonlinear unsteady aerodynamic modeling using a surrogate-based recurrence framework, AIAA Journal, vol. 48, No. 10, (2010), 2418-2429.
7. Hall, K. C., Thomas, J. P., Dowell, E. H., Proper Orthogonal Decomposition Technique for Transonic Unsteady Aerodynamic Flows, AIAA Journal, Vol. 38, No. 10, (2000), 1853-1862., doi: 10.2514/2.867
8. Haykin, S., Neural Networks a Comprehensive Foundation, Prentice-Hall Inc, second edition, 1999.
9. Huang, N. E. and Wu, Z., A review on HilbertHuang transform: Method and its applications to geophysical studies, Reviews of Geophysics, vol. 46, No. 2, (2008)
10. Landon, R. H., NACA 0012. Oscillating and Transient Pitching, *In Compendium of Unsteady Aerodynamic Measurements*, AGARD R-702, Data Set 3, 1982
11. Lindhorst, K., Haupt, M. C. and Horst, P., Efficient surrogate modelling of nonlinear aerodynamics in aerostructural coupling schemes, AIAA Journal, vol. 52, No. 9, (2014), 1952-1966.
12. Lindhorst, K., Haupt, M. C. and Horst, P., Aeroelastic Analyses of the High-Reynolds-Number-Aerostructural-Dynamics Configuration Using a Nonlinear Surrogate Model Approach, AIAA Journal, Vol. 53, No. 9, (2015), pp. 2784-2796. doi: 10.2514/1.J053743
13. Liou, M. S., A sequel to AUSM, Part II: AUSM+-up for all speeds, Journal of Computational Physics, vol. 214, No. 1, (2006), 137-170.
14. Lucia, D. and Beran, P., Reduced-Order Model Development Using Proper Orthogonal Decomposition and Volterra Theory, AIAA Journal, Vol. 42, No. 6, (2004), pp. 1181-1190.
15. Mannarino, A., Mantegazza, P., Nonlinear aeroelastic reduced order modeling by recurrent neural networks, Journal of Fluids and Structures, Vol. 48, (2014), 103-121. doi: 10.1016/j.jfluidstructs.2014.02.016
16. Nguyen, N. C., and Peraire, J., An efficient reducedorder modeling approach for nonlinear parametrized partial differential equations, International Journal for Numerical Methods in Engineering, vol. 76, No. 1, (2008), 27-55.
17. Orr, Mark, Introduction to radial basis function networks., Center for Cognitive Science, University of Edinburgh, Edinburgh TR, Scotland, U.K., 1996.
18. Rowley, C. W., Model reduction for fluids, using balanced proper orthogonal decomposition, International Journal of Bifurcation and Chaos, vol. 15, No. 3, (2005), 997-1013.
19. K.J. Badcock and M.A. Woodgate, Bifurcation Prediction of Large-Order Aeroelastic Models , AIAA Journal, vol. 48, No. 6, 2010, 1037–1046.
20. Silva, W., Identification of Nonlinear Aeroelastic Systems Based on the Volterra The-

ory: Progress and Opportunities, Nonlinear Dynamics, vol. 39, No. 1-2, (2005), 25–62, doi:10.1007/s11071-005-1907-z

21. Thomas, Jeffrey P and Dowell, Earl H and Hall, Kenneth C, Nonlinear inviscid aerodynamic effects on transonic divergence, flutter, and limit-cycle oscillations, AIAA Journal, vol. 40, No. 4, (2002), 638–646
22. Timme, S.,Marques, S. and Badcock., K., Transonic aeroelastic stability analysis using a kriging-based Schur complement formulation, AIAA Journal, vol.49, No. 6, (2011): 1202-1213.
23. Van Leer, B., Towards the ultimate conservative difference scheme. II. Monotonicity and conservation combined in a second-order scheme, Journal of computational physics, vol. 14, No. 4, (1974), 361-370.
24. Vetrano, F., Le Garrec, C., Mortchelewicz, G. D., and Ohayon, R., Assessment of strategies for interpolating POD based reduced order models and application to aeroelasticity, Journal of Aeroelasticity and Structural Dynamics 2.2, (2012).
25. Willcox, K. and Peraire, J., Balanced model reduction via the proper orthogonal decomposition, AIAA Journal, Vol. 40, No. 11, (2002), 2323-2330.
26. Xiang, C., Existence of global input-output model for nonlinear systems, In Control and Automation, 2005. ICCA'05. International Conference on. Vol. 1, pp. 125-130, (2005), IEEE.
27. Yao, W., Marques, S., Prediction of Transonic Limit Cycle Oscillations using an Aeroelastic Harmonic Balance Method, AIAA Journal, Vol. 53, No. 7, (2015), pp. 2040-2051. doi: 10.2514/1.J053565
28. Yao, W., and Liou, M.-S., A nonlinear modeling approach using weighted piecewise series and its applications to predict unsteady flows Journal of Computational Physics, Vol. 31, No. 8, 2016, pp. 58–84
29. Yao, W. and Marques, S., Model reduction for nonlinear aerodynamics and aeroelasticity using a Discrete Empirical Interpolation Method AIAA Journal, to appear
30. Yates, E. C., AGARD standard aeroelastic configurations for dynamic response I-wing 445.6, (No. AGARD-R-765), Advisory Group For Aerospace Research And Development, (1987), Neuilly-Sur-Seine (France)
31. Zhang, W., Wang, B., Ye, Z. and Quan, J., Efficient method for limit cycle flutter analysis based on nonlinear aerodynamic reduced-order models, AIAA Journal, vol. 50, No.5, (2012), 1019-1028.